ELEKTRİK, VOL.6, NO.3, 1998, ©TÜBİTAK

Imaging Tissue Conductivity via Contactless Measurements: A Feasibility Study*

Nevzat G. Gençer* and M. Nejat Tek
Department of Electrical and Electronics Engineering,
Middle East Technical University,
06531, Ankara, TURKEY
E-mail:ngencer@ed.eee.metu.edu.tr

Abstract

The feasibility of a new imaging system is investigated. This system will be used to image electrical conductivity distribution of biological tissues via contactless measurements. This will be achieved by introducing currents in the conductive medium using time-varying magnetic fields and measuring the magnetic fields of the induced currents. Consequently, the imaging system consists of transmitter and receiver coils placed nearby the conductive body. In this study, the basic features of the coplanar and coaxial coils are studied. The validity of the simplifying assumptions for the governing field equations is investigated. It is found that, for operating frequency of 100 kHz the displacement currents can be ignored, however, the propagation effects become effective for a representative distance of 20 cm. In order to estimate the induced current and the secondary field strengths, the half-space problem is solved for representative coil configurations. The validity of these solutions are also tested with a semi-analytical solution based on conductor-rings model of the half space. For coaxial coil configuration, the maximum induced current density, primary voltage and secondary voltage are obtained as 0.2×10^{-4} *mA/cm*^{2}*, 468 mV and 8.7* μ *V, respectively. These results are obtained for 1 turn transmitter coil excited by sinusoidal current having a peak value of 1 A at 50 Khz, and 10000-turn detection coil. Note that the calculated voltages are measureable while the maximum current density induced in the conductive body is much lower than the safety limits (1.6 mA/ cm*^{2}*) at that operating frequency. For coplanar coil configuration, the maximum current density increases to 4.9* $\times10^{-4}$ *mA/ cm*^{2}*, since the transmitter coil is closer to half space surface. These results ultimately revealed that the signals are in the measurable range while the currents are below the safety limits.*

1. Introduction

In this study, the feasibility of a new medical imaging modality is investigated. This modality is used to image electrical conductivity of tissues via contactless measurements. For that purpose, currents are induced in the conductive body by time-varying magnetic fields. The magnetic fields of these currents are measured by an array of coils placed nearby the body surface. By changing the location of transmitter coil, it is possible to obtain a number of measurements, which, in turn, are used to obtain conductivity distribution.

* This work was supported by Middle East Technical University Research Fund Project No: 96-03-01-01.

Simulation studies show that it is possible to obtain measurable signal levels while introducing currents below safety levels.

Fig.1 shows the general principles and data collection of magnetic-induction and magnetic field measurement system. In this method, a transmitter coil is energized by a sinusoidal current which creates a time-varying magnetic field and the electromotive force induced in a receiver coil is measured. When a conductive object is brought nearby these coils, induced currents in the object are proportional to its conductivity. These currents create secondary magnetic fields which change the voltage measured at the receiver coils.

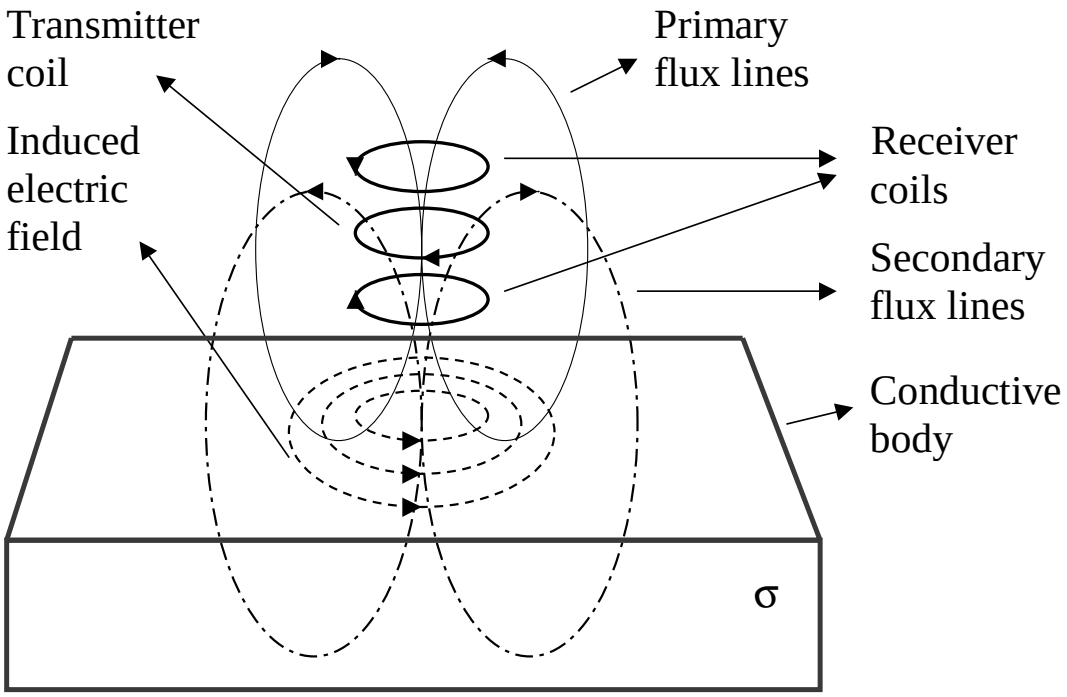

Figure 1. The general principles of magnetic-induction magnetic-measurement system

This measurement methodology has been known for about a decade and been mainly used for geophysical inspection [18]. In 1968, Tarjan and Mc Fee proposed the use of this technique for medical purpose [16], [17]. In that study, they introduced a magnetically coupled impedance measuring instrument to determine an effective electrical resistivity of human subjects. This methodology has not proceeded to become a medical imaging modality, maybe because the idea of imaging tissue properties was a new approach for medical treatment at that time. In addition, the computer technology was not well developed to provide sufficient storage and processing units. However, with the recent advent of technology, it is now possible to solve large size electromagnetic field problems using even personal computers. It is also possible to develop computer-controlled data-acquisition systems. Thus this is an appropriate time to launch an effort on the development of a medical imaging system based on induction currents and magnetic measurements using an array of transmitter and receiver coils.

Imaging the spatial distribution of conductivity or spatio-temporal evolution of conductivity changes in the human body has an important diagnostic value. Electrical impedance tomography technique has been used in characterization of cancerous tissues [1], [2], respiratory medicine [3], [4], localization of cardiac related impedance changes in the thorax [5], gastric function assessment [6], monitoring conductivity changes in the adult brain during the cardiac cycle [7], in thermal monitoring of hyperthermia treatment [8] and in the

localization of epileptic foci [9]. In addition to these applications, conductivity values of tissues are required to develop realistic electrical models of the human body. This increases accuracy in finding electrical sources in the brain [14] and heart [15]. Modern imaging modalities provide high resolution images which can be processed by state-of-the-art segmentation algorithms to classify the different tissues. However, realistic models still require accurate conductivity values for tissues.

Different methods have been proposed to obtain static or dynamic conductivity images of the human body. In applied-current electrical impedance tomography (ACEIT), low frequency sinusoidal currents are applied via electrodes attached to the body surface. In induced-current (ICEIT), currents are induced into the body by time-varying magnetic fields (e.g., 50kHz) [19], [24], [20], [21], [22]. The limitations of current injection from the surface electrodes are discussed in detail in [19] and [22]. One major disadvantage of current injection is the screening effect of superficial insulating tissue layers, such as bone. This is especially important for head applications. However, in induced current EIT, it is possible to couple currents into deep-lying tissues. An important problem in both techniques is the attachment of electrodes on the body surface to measure the voltage differences. In order to increase the measurements, one has to increase the number of electrodes attached on the body surface. However, electrode placement and recording their precise locations are important problems in practice [27]. Consequently, an imaging methodology that uses time varying magnetic fields to couple currents in the conductive media and makes contactless measurements by receiver coils seems to have a potent for applications in biomedicine.

The feasibility of the measurement system can be explored by using the relations for 1) the induced currents in a conductive body due to a source current in an transmitter coil and 2) the magnetic fields due to the induced currents. These expressions can be considerably simplified depending on the material's electrical properties, size of the survey area and the operating frequency. For that purpose, we shall begin with the basic electromagnetic theory governing the sinusoidally varying currents and fields (The topics covered in this section can be found elsewhere [29],[30]. The next section provides a method based on $\mathbf{A}-\phi$ formulation for the solution of secondary magnetic fields due to the induced currents in the conductive medium. The following section is on the tissue electrical characteristics. The validity of several simplifying assumptions are also discussed in that section. The half-space problem and the related field expressions are introduced in the last section.

2. Basic Electromagnetic Theory

The following set of Maxwell's equations govern the behavior of the sinusoidally varying (e^{jwt} time-dependence is assumed) electromagnetic fields in a linear, nonmagnetic, isotropic conductive medium [29]:

$$\begin{aligned} \nabla \times \mathbf{E} &= -j\omega\mu\mathbf{H} & \nabla \cdot \mathbf{D} &= \rho \\ \nabla \times \mathbf{H} &= \sigma\mathbf{E}+j\omega\epsilon\mathbf{E} & \nabla \cdot \mathbf{B} &= 0 \end{aligned}$$

with the continuity equation

$$\nabla \cdot \mathbf{J} = -j\omega\rho \tag{1}$$

and the following relations

$$\begin{aligned} \mathbf{D} &= \epsilon\mathbf{E} \\ \mathbf{J} &= \sigma\mathbf{E} \end{aligned} \tag{2}$$

$$\mathbf{B} = \mu\mathbf{H} \tag{3}$$

The symbols $\mathbf{E}$, $\mathbf{D}$, $\mathbf{H}$ and $\mathbf{B}$ are the electric field, electric displacement, magnetic field intensity and magnetic flux density in complex phasor notation, respectively. Here the radial frequency is denoted by ω and charge density is denoted by ρ. The material constants, namely, conductivity, permittivity and permeability are represented by σ, ϵ and μ, respectively.

By algebraic recombination of these equations we obtain the following Helmholtz equations:

$$\nabla^2\mathbf{E} - k^2\mathbf{E} = 0 \tag{4}$$
$$\nabla^2\mathbf{H} - k^2\mathbf{H} = 0 \tag{5}$$

where the quantity

$$k^2 = (j\omega\mu\sigma - \omega^2\epsilon\ \mu) \tag{6}$$

is the square of the wave number k that depends on the material constants and operation frequency. The wave number k has both real and imaginary parts which can be expressed as

$$k = \alpha + j\beta \tag{7}$$

where

$$\alpha = \left[\frac{\omega\mu\sigma}{2}\left((1 + \frac{\omega^2\epsilon^2}{\sigma^2})^{1/2} - \frac{\omega\epsilon}{\sigma}\right)\right]^{1/2} \tag{8}$$
$$\beta = \left[\frac{\omega\mu\sigma}{2}\left((1 + \frac{\omega^2\epsilon^2}{\sigma^2})^{1/2} + \frac{\omega\epsilon}{\sigma}\right)\right]^{1/2}. \tag{9}$$

Here α is the attenuation constant and β is a measure of the radian phase shift per meter (the phase constant). The wavelength λ and the skin depth δ (the distance the wave must propagate in order to decay by an amount e^{-1}) are defined as:

$$\lambda = \frac{2\pi}{\beta} \tag{10}$$
$$\delta = \frac{1}{\alpha}. \tag{11}$$

.

If the displacement currents ($j\omega\epsilon\mathbf{E}$) are negligible compared to conduction currents ($\sigma\mathbf{E}$), in other words if $\omega\epsilon/\sigma \ll 1$, then the wave number can be written as

$$k = (j\omega\sigma\mu)^{1/2}. \tag{12}$$

The alternative forms are

$$k = (\sigma\omega\mu/2)^{1/2}(1 + j) = (1 + j)/\delta \tag{13}$$

The skin depth under this assumption is

$$\delta = (\frac{2}{\omega\mu\sigma})^{1/2}. \tag{14}$$

For a piecewise conductive medium, the electric charges can exist at the interfaces of different conductive regions. Within the uniform pieces the volume charge density is zero. Then for each region the following system of equations is satisfied

$$\begin{array}{rclcrcl} \nabla \times \mathbf{E} & = & -j\omega\mu\mathbf{H} & & \nabla \cdot \mathbf{E} & = & 0 \\ \nabla \times \mathbf{H} & = & \sigma\mathbf{E} & & \nabla \cdot \mathbf{B} & = & 0 \end{array}.$$

with the continuity equation

$$\nabla \cdot \mathbf{J} = 0$$

3. Forward Problem Solution

The forward problem can be defined as solving the secondary magnetic fields due to induced currents in a conductive body. In order to calculate the secondary magnetic fields, the electric field in the conductive body must be solved due to a current carrying transmitter coil nearby the conducting body. In this section we shall present a method based on $\mathbf{A} - \phi$ formulation of the electric field.

Since the magnetic field density $\mathbf{B}$ has zero divergence, it can be expressed as a curl of a vector field, i.e., $\mathbf{B} = \nabla \times \mathbf{A}$ where $\mathbf{A}$ is known as magnetic vector potential [29]. $\mathbf{A}$ is an auxilary vector field which is usually used to calculate the electric field $\mathbf{E}$ more conveniently. Using $\nabla \times \mathbf{A}$ in place of $\mathbf{B}$, we obtain

$$\begin{aligned} \nabla \times \mathbf{E} &= -j\omega\nabla \times \mathbf{A} \\ \nabla \times (\mathbf{E} + j\omega\mathbf{A}) &= 0. \end{aligned} \tag{15}$$

Since curl of a gradient of a scalar function is zero

$$\mathbf{E} + j\omega\mathbf{A} = -\nabla\phi \tag{16}$$

where ϕ is named as scalar potential function. Consequently,

$$\mathbf{E} = -j\omega\mathbf{A} - \nabla\phi \tag{17}$$

which shows that the electric field has two sources: change of the magnetic field with time, and surface and volume charges. The electric field $\mathbf{E}$ can be calculated by solving the following coupled equations:

$$\nabla \times \nabla \times \mathbf{A} = \mu\sigma(-j\omega\mathbf{A} - \nabla\phi) + \mu\mathbf{J} \tag{18}$$

$$\nabla \cdot (j\omega\sigma\mathbf{A} + \sigma\nabla\phi) = 0. \tag{19}$$

According to the Helmholtz theorem, a vector function is completely specified if its divergence and curl are known. The partial differential equations governing the behavior of $\mathbf{A}$ are considerably simplified with the choice of Lorentz gauge [31], that is

$$\nabla \cdot \mathbf{A} = -\mu\sigma\phi \tag{20}$$

so that

$$\nabla(\nabla \cdot \mathbf{A}) = -\mu\sigma\nabla\phi. \tag{21}$$

With this gauge condition we obtain a Helmholtz equation for the magnetic vector potential,

$$\nabla^2\mathbf{A} - k^2\mathbf{A} = -\mu\mathbf{J} \tag{22}$$

where $\mathbf{J}$ is the current density, for example, in a current carrying transmitter coil. Solution of (22) is

$$\mathbf{A} = \frac{\mu}{4\pi}\int \frac{\mathbf{J}e^{-jkR}}{R}dV \tag{23}$$

where R is the distance between the current source and field points, and V denotes the volume of current sources.

If the region of interest is nearby the sources and if the extent of the source is smaller than the wavelength then the propagation effects can be assumed to be negligible. In other words, the e^{-jkR} term in the integrand can be replaced by unity and the solution for $\mathbf{A}$ reduces to the one obtained for static case

$$\mathbf{A} = \frac{\mu}{4\pi}\int \frac{\mathbf{J}}{R}dV. \tag{24}$$

Note that the magnetic vector potential $\mathbf{A}$, obtained in this way, is the primary field that exists when the conductive object is not present; in other words the effects of the conductive object are ignored. Once $\mathbf{A}$ is calculated ϕ can be obtained for an assumed conductivity distribution by solving the following partial differential equation [21]:

$$\nabla \cdot (\sigma\nabla\phi) = -\nabla\sigma \cdot j\omega\mathbf{A} \tag{25}$$

$$\sigma\frac{\partial\phi}{\partial n} = -j\omega A_n \tag{26}$$

where n represents the outward normal and A_n is the normal component of $\mathbf{A}$ on the surface of the conductive medium. After finding the components of $\mathbf{E}$, the induced current density $\mathbf{J}_i$ can simply be obtained by

$$\mathbf{J}_i = \sigma(-j\omega\mathbf{A} - \nabla\phi) \tag{27}$$

These currents are the basis of secondary magnetic field $\mathbf{B_s}$ that reflect the properties of the conductive object. $\mathbf{B_s}$ can be calculated by using the Biot-Savart Law:

$$\mathbf{B_s} = \frac{\mu_0}{4\pi}\int \frac{\mathbf{J}_i \times \mathbf{R}}{R^3}dV \tag{28}$$

where μ_0 is the free space permeability, R is the distance between the source point in the conductive medium to the field point and V represents the conductive medium volume.

In practice $\mathbf{A}$ can be calculated using numerical integration for a general coil geometry. For objects of arbitrary conductivity distribution ϕ can be obtained by solving the related partial differential equation

using numerical procedures, like the Finite Element Method (FEM). FEM formulations for solving ϕ in two- and three-dimensional body geometries have been given in [21] and [23]. Thus using these numerical procedures the induced current density in the conductive medium can be evaluated. The secondary magnetic fields $\mathbf{B_s}$, as given by (28), can then be obtained by numerical integration.

Note that in the above given formulation there are two basic assumptions: 1) the displacement currents are neglible, 2) the propagation affects are negligible. The validity of these assumptions depends on the operation frequency, electrical properties of the medium and the maximum survey distance (the maximum distance between the transmitter-receiver array and the conductive body). The next section explores the validity of these assumptions.

4. Useful Assumptions

4.1. Effects of displacement currents

Most of the biological tissues have permeability close to that of the free space (i.e., $\mu = \mu_0 = 4\pi \times 10^{-7}$ Henry/m). However, they have different dielectric constants and electrical conductivities. Moreover these electrical properties change with frequency. The dielectric constant of biological tissues decreases with increasing frequency [12]. The electrical conductivity is, however, very weakly dependent on frequency and may be thought of constant between 10 Hz and 10 MHz [32], [13]. The mean conductivities of different tissues are listed in Table 1 as reported by Rush *et al.* [11].

The current $\mathbf{J}$ in the conductive medium is the sum of two components: the conduction current $(\sigma\mathbf{E})$ and the displacement currents $(j\omega\epsilon\,\mathbf{E})$. For a particular frequency, the ratio $\omega\epsilon/\sigma$ determines the importance of displacement currents relative to conduction currents. If this ratio is small for majority of the tissues, then the medium can be assumed resistive and it is possible to use the simplified form of the Maxwell's equations. .

Note that in most of the Electrical Impedance Tomography (EIT) studies in the literature the displacement currents are neglected if the the operation frequency is below 100 kHz [32]. In this study, the validity of this assumption is tested by calculating $\omega\epsilon/\sigma$ for various tissue types at different frequencies up to 150 kHz (Table 2). The dielectric constants and conductivity values are compiled from [10] and a number of secondary sources [33], [34], [35]. It is observed that, apart from certain tissues like, heart muscle, kidney, liver and lung, the displacement currents can be assumed negligible compared to the conduction currents for frequencies below 100 kHz.

Table 1. Electrical Conductivity of Biological Tissues

Tissue	Mean conductivity (Siemens/m)
Blood	0.67
Lung	0.05
Liver	0.14
Fat	0.04
Human trunk	0.21

Table 2. Ratio of Displacement to Conduction Currents for Various Frequencies and Body Tissues

	10 Hz	100 Hz	1 kHz	10 kHz	40.96 kHz	100 kHz	150 kHz
Lung	0.15	0.025	0.05	0.14	0.422	-	-
Fat		0.01	0.03	0.15	0.020	0.015	0.019
Liver	0.20	0.035	0.06	0.20	0.331	0.529	0.579
Heart Muscle	0.10	0.04	0.15	0.32	-	-	-
Sceletal muscle, longitudinal	0.0069	0.0153	0.0556	-	0.036	0.190	0.215
Sceletal muscle, transverse	0.01	0.12	0.7	-	-	-	-
Bone	-	-	0.008	0.053	0.151	0.107	0.133
Kidney	-	-	-	-	0.309	0.385	0.402
Spleen	-	-	-	-	0.093	0.0297	0.040

Table 3. Wavelengths and Skin Depths for Various Frequencies

Frequency (kHz)	λ(m)	$\delta(m)$
1	143.91	55.30
10	45.51	17.48
50	20.35	7.82
100	14.39	5.53

Table 4. Propagation Related Parameters for Various Frequencies. The error Column shows the Percentage error From Unity. Magnitude and phase Difference (P) of e^{-jkR} is tabulated.

	R = 20 cm			R = 10 cm		
Frequency (kHz)	$\lvert e^{-jkR}\rvert$	P(^{o})	error(%)	$\lvert e^{-jkR}\rvert$	P(^{o})	error(%)
1	0.9921	0.46	0.79	0.9960	0.22	0.40
10	0.9752	1.44	2.48	0.9875	0.72	1.25
50	0.9454	3.22	5.46	0.9723	1.61	2.77
100	0.9236	4.55	7.64	0.9610	2.27	3.90

4.2. Effects of e^{-jkR} term

At a frequency of 100 kHz the wavelength in free space is 3000 m. Thus for a survey distance of 20 cm the propagation effects (or the e^{-jkR} term) can certainly be neglected. However, the validity of this assumption is questionable if the field is to be calculated in biological tissues (since they have considerable conductivity and permitivity values). For an average tissue conductivity of (0.2 Siemens/m) and in the same survey distance ($R_{max} = 0.2$ m) , the wavelengths and skin depths for different frequencies are given in Table 3. Table 4 presents propagation related parameters; magnitude and phase of e^{-jkR}. In both of these tables, the associated parameters are obtained by setting $\omega\epsilon/\sigma$ ratio to a conservative value of 1. It can be observed that for an operating frequency of 10 kHz, the percentage error between the magnitude of e^{-jkR} and unity is negligible (2.48%) whereas this error seems more significant (7.64%) for 100 kHz. Note that $\omega\epsilon/\sigma$ ratio is smaller than unity for all tissues between 0-150 kHz range. Even for liver at 100 kHz the ratio $\omega\epsilon/\sigma = 0.5293$, and the percentage error is only 5.3%. Consequently, we can conclude that e^{-jkR} term can be neglected up to 100 kHz in biological tissues.

5. Sample Problem

Wait has derived field expressions for multi-layer half-space earth excited by a circular coil located in the air (Fig. 2), for the purpose of geophysical exploration [18]. In that study, rather simple formulations are obtained using the two basic assumptions we have discussed in the preceding section (displacement currents are and propagation effects are negligible). As long as the same assumptions hold, the same formulations can be used to understand the feasibility of a measurement system to measure the tissue conductivity.

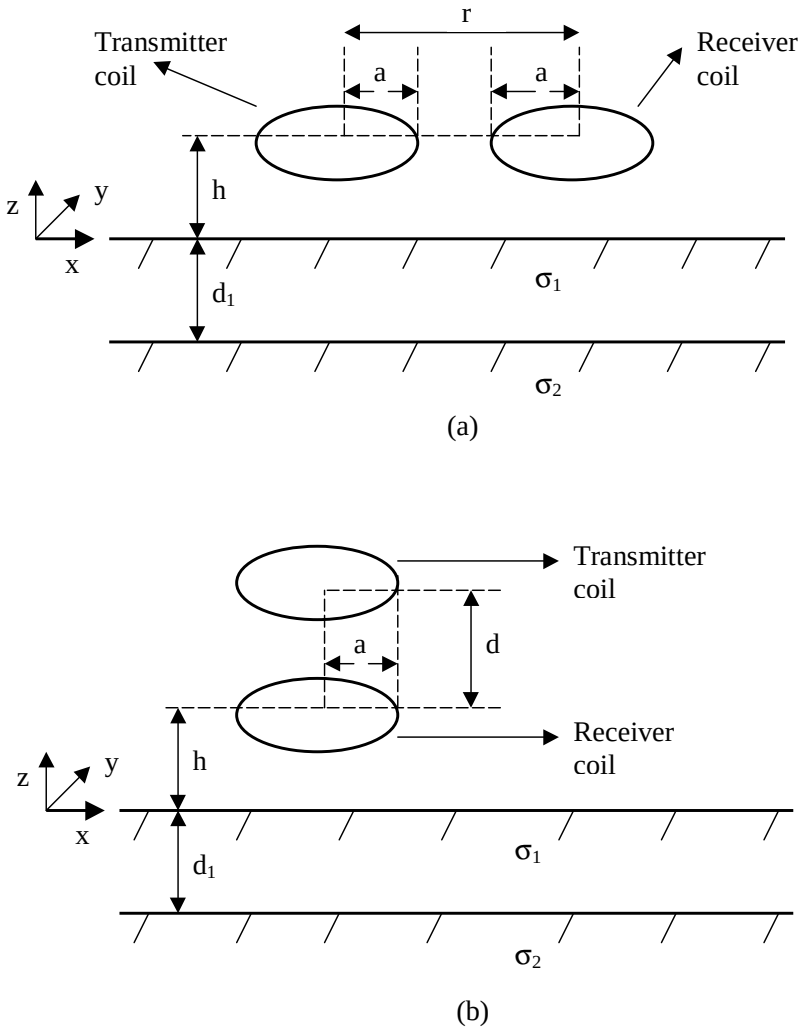

Figure 2. Circular loop over two-layer half-space

In this section we shall first summarize Wait's formulation to provide the reader a perspective about the field equations for a simple coil-body geometry. The secondary magnetic fields and the induced current density values will be calculated for representative coil configurations. In order to verify the solutions, the results will be compared with the solutions of a semi-analytical method proposed in this study.

5.1. Analytical Solution

In the source-free air region nearby the conductive body $\nabla \times \mathbf{H} = 0$. Thus $\mathbf{H}$ can be expressed as a gradient of a scalar funtion $\mathbf{H} = -\nabla\Phi$ in the air. In addition, since $\nabla \cdot \mathbf{H} = 0$, the fields in the air are derivable from

the solution of Laplacian equation

$$\nabla^2\Phi = 0$$

together with the appropriate boundary and interface conditions. As a specific example, Fig.2 shows transmitter and receiver coils placed over a two-layer conductive medium of infinite extent. For $z > 0$, the magnetic scalar potential Φ can be expressed as a sum of primary Φ_p and secondary Φ_s potentials, where Φ_p is the potential when the two-layer conductive medium does not exist. Note that both Φ_p and Φ_s satisfy Laplacian equation and simple analytical solutions exist for special object and coil geometries using appropriate boundary conditions at the air-body interface.

Wait's formulations yields rather simple expressions for the primary and secondary magnetic field expressions in the air region (i.e., for $z > 0$):

$$\begin{aligned} H_x^p &= 3Cx(z-h)/R^5 \\ H_y^p &= 3Cy(z-h)/R^5 \\ H_z^p &= 3C(z-h)^2/R^5 - C/R^3 \end{aligned}$$

$$\begin{aligned} H_x^s &= -Ct_1(x/r) \\ H_y^s &= -Ct_1(y/r) \\ H_z^s &= -Ct_0 \end{aligned}$$

where $R = (r^2+(z-h)^2)^{1/2}$, $C = IdA/4\pi$ and $dA = \pi a^2$ the infinitesimal area of the coil. The parameters t_0 and t_1 are defined as

$$\begin{aligned} t_0 &= \frac{k_1^2}{4}\left\{\frac{1}{[r^2+(z+h)^2]^{1/2}} - \frac{1}{[r^2+(2d+z+h)^2]^{1/2}}\right\} + \frac{k_2^2}{4}\left\{\frac{1}{[r^2+(2d+z+h)^2]^{1/2}}\right\} \\ t_1 &= \frac{k_1^2}{4r}\left\{\frac{2d+z+h}{[r^2+(2d+z+h)^2]^{1/2}} - \frac{z+h}{[(2d+z+h)^2]^{1/2}}\right\} - \frac{k_2^2}{4r}\left\{\frac{z+h}{[(2d+z+h)^2]^{1/2}}\right\} \end{aligned} \quad . \tag{29}$$

Here $k_1^2 = j\omega\mu_0\sigma_1$ and $k_2^2 = j\omega\mu_0\sigma_2$. The basic assumptions leading to these simple expressions are: 1) the radius of the coil is vanishingly small (thus we deal here with a magnetic dipole), 2) the displacement currents are negligible, i.e., $\omega\epsilon_1 \ll \sigma_1$ and $\omega\epsilon_2 \ll \sigma_2$, and 3) $\mid k_1^2R \mid^2 \ll 1$ and $\mid k_2^2R \mid^2 \ll 1$.

Similar geometry and coil configuration can be used to understand field quantities assuming the conductive body under exploration has biological tissue properties. For instructive purposes, we shall follow Wait's mutual impedance (Z) formulation [18] that relates the voltages in the receiver coil due to the current in the transmitter coil. The derivations of two types of coil configurations (as given in Fig. 2) will be presented: 1) coplanar coils with axes vertical to the half space, and 2) coaxial coils with axes vertical to the half space. We shall then calculate the primary and secondary voltages and fields for representative coil configuration parameters in order to have an insight about the field magnitudes.

5.1.1. Coplanar coils with axes vertical to the half space

Let the transmitter coil area, the number of turns and the coil current be denoted by S_1, N_1, and I, respectively. Since both coils are at the same height ($z = h$), the first term of the primary magnetic field H_z^p is zero. Thus H_z^p at a distance r is

$$H_{z,copl}^p = -\frac{IN_1S_1}{4\pi r^3}. \tag{30}$$

The primary voltage v_p induced in a N_2-turn receiver coil of area S_2 is

$$v_p = -j\omega(\mu_0 H^p_{z,copl}) \times N_2 S_2. \tag{31}$$

Thus the mutual impedance (Z^p_{copl}) for coils located in free space is:

$$Z^p_{copl} = \frac{v_p}{I} = j\omega\mu_0 \frac{(N_1 S_1) \times (N_2 S_2)}{4\pi r^3}. \tag{32}$$

A similar formulation can be derived to calculate the mutual impedance $Z_{copl} = Z^p_{copl} + Z^s_{copl}$ between coils over layered half-space. Here Z^s_{copl} represents the contribution of the induced currents in the conductive half-space. The secondary voltage v_s can be calculated by

$$v_s = -j\omega(\mu_0 H^s_z) \times N_2 S_2 \tag{33}$$

where $H^s_z = -(IN_1 S_1/4\pi) \times t_0$. Consequently, we obtain

$$Z^s_{copl} = \frac{v_s}{I} = j\omega\mu_0 \frac{(N_1 S_1) \times (N_2 S_2)}{4\pi} \times t_0 = Z^p_{copl}\ r^3 \times t_0 \tag{34}$$

and

$$Z = Z^p_{copl}(1 + r^3 t_0). \tag{35}$$

For illustrative purposes, the primary and secondary fields and voltages are calculated for a coil of radius $a =$ 1 cm, located at a height of $h = 1$ cm from a uniform conductor of conductivity $\sigma = 0.2$ Siemens/m. (i.e., $\sigma_1 = \sigma_2 = \sigma$). The transmitter coil carries sinusoidal current at 1 kHz. The receiver coil is assumed to be at the same height from the conductive half-space and located at a distance of $r = R = 5$ cm. in order to approximate the transmitter coil as a magnetic dipole. Both receiver and transmitter coils are initially assumed to be 1 turn (i.e., $N_1 = N_2 = 1$). For such a coil configuration, the mutual impedances are found as Z^p_{copl}= j0.5 μV/A and Z^s_{copl}=-0.45 pV/A, respectively. Note that these values considerably increase when the operating frequency becomes 50 kHz and the number of turns of the receiver coil increases to $N_2 = 10000$. For such a configuration, Z^p_{copl}= j0.25 V/A and Z^s_{copl}=-11.4 μV/A, respectively. The maximum current density is found as 4.9×10^{-4}mA/cm^2. The $|\, kR\,|^2$ values are on the order of 10^{-8} and 10^{-5} for 1 kHz and 50 kHz operating frequency, which are much smaller than unity.

5.1.2. Coaxial coils with axes vertical to the half space

The primary magnetic field $H^p_{z,coax}$ at a distance d from the transmitter coil center is

$$H^p_{z,coax} = \frac{IN_1 S_1}{2\pi(a^2 + d^2)^{3/2}} \tag{36}$$

The primary voltage v_p induced in an N_2-turn receiver coil of area S_2 is in the form of equation (31):

$$v_p = -j\omega(\mu_0 H^p_{z,coax}) \times N_2 S_2. \tag{37}$$

Thus the mutual impedance (Z^p_{coax}) for coaxial coils located in free space is:

$$Z^p_{coax} = \frac{v_p}{I} = -j\omega\mu_0 \frac{z(N_1 S_1) \times (N_2 S_2)}{2\pi(a^2 + d^2)^{3/2}}. \tag{38}$$

The secondary voltage is in the form of (33) leading to

$$\begin{aligned} Z^s_{coax} &= \tfrac{1}{4\pi} j\omega\mu_0 (N_1 S_1) \times (N_2 S_2) \times t_0 \\ &= -\tfrac{1}{2} Z^p_{coax}\ (a^2+d^2)^{3/2} \times t_0 \end{aligned} \tag{39}$$

and

$$Z_{coax} = Z^p_{coax}\ [1 - \frac{1}{2}(a^2+d^2)^{3/2} \times t_0].$$

As in the coplanar coil case, the signal strengths will be calculated for a representative coil configuration. The transmitter coil of radius 1 cm ($a = 1$ cm) is located at 6 cm from the conductive half space ($h = 6$ cm). The number of turns of the transmitter and receiver coils is taken as 1 ($N_1 = 1,\ N_2 = 1$). The transmitter coil carries sinusoidal current at 1 kHz. The receiver coil is of the same size with the transmitter coil and located 1 cm above the conducting object. For such a coil configuration, the mutual impedances are $Z^p_{coax} = 0.6$ nV/A and $Z^s_{coax} = 0.04$ pV/A, respectively. The maximum induced current density is obtained as 4.15 μA/m^2 at $r = 4.5$ cm on the surface of the half space. However, when we increase the operating frequency to 50 kHz and take $N_2 = 10000$, we obtain primary and secondary voltages as $v_p = 468$ mV and $v_s = 8.7\,\mu$V, respectively. The maximum current density is now increased to 0.2×10^{-4} mA/cm^2 at $r = 4.5$ cm.

5.2. Semi-Analytical Solution

5.2.1. Isolated- Ring Problem

Fig. 3 shows a conductor ring of cross sectional area Δ^2, conductivity σ and radius P below a coaxial coil configuration. We shall first derive the currents induced in the conductor ring caused by the sinusoidal current in the transmitter coil. The magnetic vector potential A_ϕ at point (P, L+h) is given by

$$A_\phi = \frac{\mu_0 I}{\pi k}(\frac{a}{P})^{1/2}\left[(1-\frac{1}{2}k^2)K(k^2) - E(k^2)\right] \tag{40}$$

where

$$k^2 = \frac{4aP}{[(a+P)^2+(L+h)^2]^{1/2}}.$$

For sinusoidal excitation, the electric field E_ϕ is

$$E_\phi = -j\omega A_\phi.$$

Then the current density is $J_\phi = \sigma E_\phi$ and current in the conductor ring is $I_{in} = \Delta^2 J_\phi$. This leads to the following expression:

$$I_{in} = -\frac{j\omega\sigma\mu_0\Delta^2 I}{2\pi P}\left[(a+P)^2+(L+h)^2\right]^{1/2} \times \left[(1-\frac{1}{2}k^2)K(k^2) - E(k^2)\right]. \tag{41}$$

Once the induced current strength I_{in} in the conductor ring is known, it is easy to calculate the secondary electric field E^s_ϕ that occur on the receiver coil of radius b:

$$E_\phi^s = -\frac{j\omega\mu_0 I_{in}}{\pi k}(\frac{P}{b})^{1/2}\left[(1-\frac{1}{2}k^2)K(k^2)-E(k^2)\right]$$

where k^2 is now modified to

$$k^2 = \frac{4Pb}{[(P+b)^2+(h)^2]^{1/2}}.$$

The secondary voltage v_s can be calculated by integrating E_ϕ^s on the coil contour. Since E_ϕ^s is constant on the circular coil, integration corresponds to a multiplication by $2\pi b$, which leads to

$$v_s = -j\omega\mu_0 I_{in}\left[(P+b)^2+(h)^2\right]^{1/2}\times\left[(1-\frac{1}{2}k^2)K(k^2)-E(k^2)\right]. \quad (42)$$

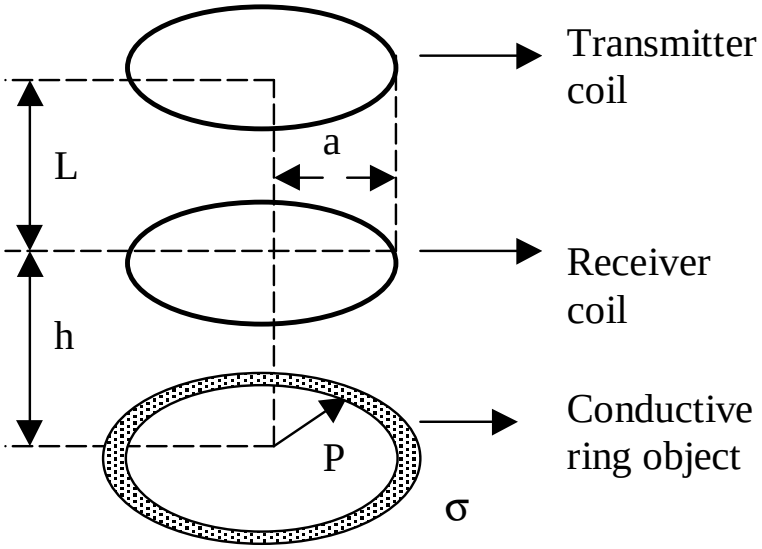

Figure 3. Conductor ring under coaxial transmitter and receiver coils

5.2.2. Half-Space Problem

An approximate solution for the half-space problem defined in Fig. 2 (b) can be obtained by representing the semi-infinite half-space with coaxial conductor rings as shown in Fig. 4. Note that the time-varying current in the transmitter coil induces currents in each conductor ring. In addition, the currents in these rings will interact with each other. Assuming such interaction to be negligible compared to the currents induced by the transmitter coil, it is possible to find an approximate solution for the secondary magnetic fields. The analytical formulation obtained for the isolated-ring problem can be used to find the induced current in each ring and its contribution to the total secondary magnetic field. The results can be compared to the solutions obtained by Wait's analytical formulations 1) to check the order of magnitudes of the field strengths, and 2) to understand whether the interaction between the conducting rings are indeed negligible.

Analytical formulation is evaluated for the representative values, transmitter coil height is $L+h=6$ cm, receiver coil height h =1 cm, receiver radius and transmitter radius a =1 cm and conductive half space conductivity 0.2 S/m. The half space is assumed to be a cylinder of height 30 cm and radius 50 cm. These dimensions are chosen as rings of larger radii and rings at greater depth produce negligible contribution to the secondary fields at the receiver coil. The cross section of each ring has a diameter of 2 mm. For this

configuration, the secondary voltage in the pickup coil is found to be 7.43 μV. For the same configuration Wait's analytical formulation yields a pickup voltage of 8.74 μV. Taking the result of Wait's formulation as a reference, the percentage error introduced by the isolated-rings model of the half space is around 15 %.

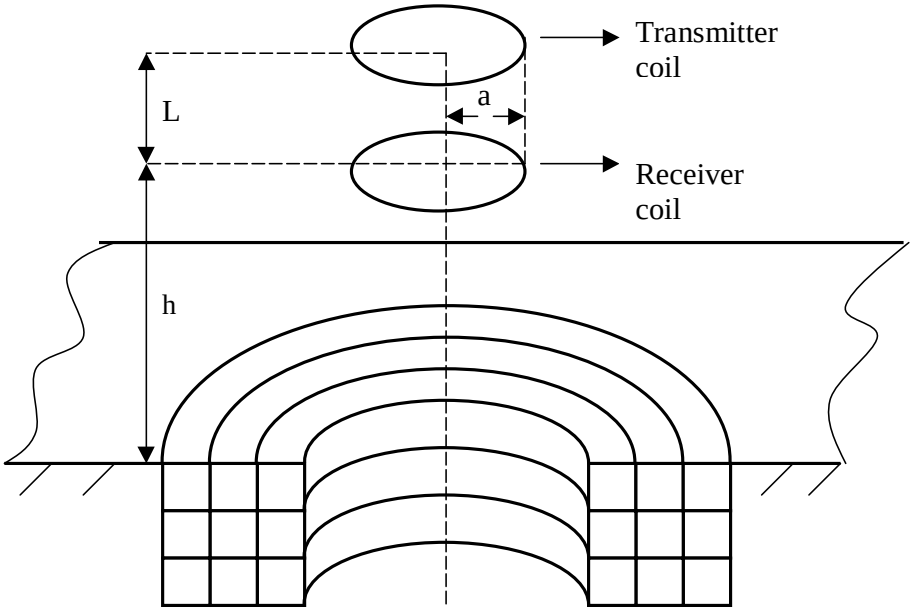

Figure 4. Coaxial coils over conducting half-space. The half space is modeled with coaxial conducting rings.

The results obtained by analytical and semi-analytical solutions verify the order of magnitude of the measurements for that specific coil configuration and operating frequency (i.e., the measurements are on the order of microvolts). In addition, it is observed that the interaction of currents in the conductive body can produce a significant difference in the calculated voltages. However, this behavior strongly depends on the operating frequency.

6. Conclusion

In this study, the feasibility of a new medical imaging modality was explored. This modality provides tissue conductivity distribution via contactless measurements. This is achieved by inducing currents on the body using time-varying magnetic fields and measuring the magnetic fields of the induced currents . This study was made to reveal whether magnetic measurements are observable while the induced currents are below the safety levels. For that purpose, the governing field equations were introduced, the simplifying assumptions were investigated and a numerical method was proposed for the solution of the forward problem.

In general, the diplacement currents can be assumed negligible if the operation frequencies are less than 100 kHz. However, if the medium has the electrical characteristics of specific tissues like heart muscle, kidney, liver and lung then the operation frequency should be smaller than 40 kHz. Note that the overall effect of all body tissues may be best observed by making *in vivo* experiments. Tarjan had compared the phase shift in magnetic measurements for a column of salt water ($\omega\epsilon = 2\pi \times 10^5 \times 78.2 \times 8.82 \times 10^{-}12 = 4.34$ Siemens/ m, $\sigma = 0.2$ Siemens/m) and human torso [16]. He has found that the phase shift is within ± 3 degrees for both salt water and the human torso. Thus Tarjan had concluded that human body acts like a salt water column and assumed the displacement currents are negligible at 100 kHz. However, Tarjan's measurements were obtained using large size pickup coils to obtain average resistivity of human torso. For

imaging purposes, with spatially localized magnetic field sensors, the measurements will be sensitive to a smaller area for which the local tissue properties may not allow the neglection of displacement currents at that frequency.

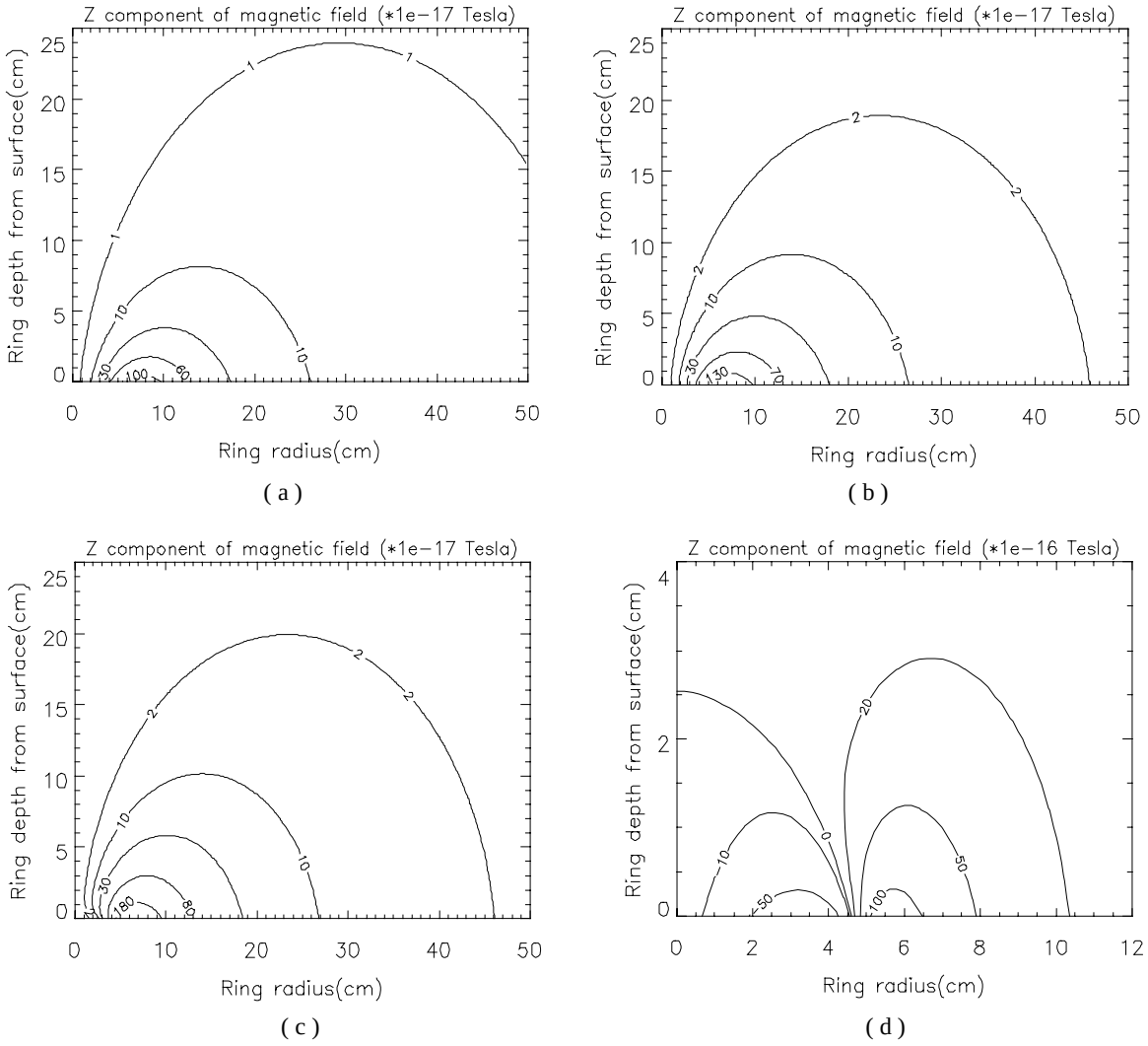

Figure 5. Contribution of conductor rings on the secondary magnetic fields. The contribution of each ring is calculated and displayed on the pixel coordinates (ring radius, ring depth) for various transmitter coil heights h. (a) h=5 cm, (b) h=4 cm (c) h=3 cm, (d) h=1 cm.

The propagation effects are found negligible for a survey distance of 20 cm if the operation frequency is less than 100 kHz. The validity of this assumption should be checked for higher operation frequencies or larger survey distances.

The closed form magnetic field expressions, derived for conducting half-space, constituted the basics of this study. The field strengths and pick-up voltage levels were obtained for a representative coil configuration (coaxial and coplanar) when the coils were above a half space of average tissue conductivity. The pick-up voltages were on the order of microvolts for representative configurations while the maximum induced currents were much lower than the safety levels at operation frequency of 50 kHz. The order of magnitudes

of the solutions was also tested by a semi-analytical solution based on isolated-rings model of the half-space developed in this study.

Biological tissue geometries are different than those of half-planes or rings. In addition, the electrical conductivity distribution in human body is inhomogeneous. Consequently, an estimate for the induced current density in biological tissues can be obtained by using complicated numerical models.

The performance of the measurement system can be enhanced by adjusting different parameters like operating frequency, coil sizes, number of turns of transmitter and receiver coils, current in the transmitter coil, and distance to the conductive object. Note that there is 90° phase difference between the primary and secondary voltages, thus phase sensitive detectors can be used to enhance the S/N ratio. Modern lock-in amplifiers with input signal sensitivity on the order of nanovolts can be utilized to increase the accuracy in measurements. However, first the relatively large primary voltages must be eliminated by a proper differential coil system [16] (or by other means) to obtain a better sensitivity to the secondary voltages. The ratio between the primary and secondary voltages is approximately 20,000:1. In order to reveal the data the primary voltages must be properly eliminated. If the secondary voltages are to be measured with an accuracy of 1% then the primary voltages must be cancelled by at least one part in 2 million. Note that, in an older study, cancellation of one part in 10 million had already been achieved by manual adjustments (Tarjan and Mc Fee, 1968). An automatic calibration mechanism should be developed if an array of coils is to be used for imaging purposes.

The elimination of possible noise sources, the use of multi-frequency excitations, the maximum allowable survey distance, and data-acquisition time are topics of possible future studies.

7. Appendix

7.1. Safety Considerations

Any medical device must obey strict safety standards set by national or international organizations. These standards are for both low-frequency leakage currents and the currents required for the normal operation of the system. In [36] the standards of four organizations were listed and it was concluded that, a maximum current of 5 mA rms can be allowed for current injection at operating frequency of 50 kHz. Assuming that this current is applied to body using ECG electrodes of area 3 cm^2 the maximum allowable current density $\mathbf{J}_{max}$ is found as 1.6 mA/cm^2.

Note that the threshold current strength for sensation increases linearly with frequency [37]. For operating frequency of 100 kHz $\mathbf{J}_{max}$ will be 3.2 mA/cm^2. Tarjan and Mc Fee had developed a system to measure average resistivity of head and torso based on magnetic induction and magnetic measurements [16]. Their system was operating at 100 kHz and the maximum current density that was applied to human head was 2.2 mA/cm^2. Their subjects have reported no sensation of nerve stimulation or heating at any part their body as expected.

References

[1] B. D. Sollish, E. H. Frei, E. Hammerman, S. B. Lang, M. Moshitzky, Microprocessor-assisted screening techniques, *Isr. J. Med. Sci.*, 17, 859-864, 1981

[2] G. Piperno, E. H. Frei,M. Moshitzky, Breast cancer screening by impedance measurements *Frontiers Med. Biol. Eng.* 2(2), 111-117, 1990

[3] N. D. Harris, A. J. Suggett, D. C. Barber, B. H. Brown, Applications of applied potential tomography (APT) in respiratory medicine, *Clin. Phys. Physiol. Meas.* Vol. 8, Suppl. A, 155-165, 1987

[4] L. A. W. Smulders, A. van Oosterom, Application of electrical impedance tomography to the determination of the lung volume, *Clin. Phys. Physiol. Meas.* Vol. 13, Suppl. A, 167-170, 1992

[5] B. M. Eyuboglu, B. H. Brown, D. C. Barber, A. D. Seagar, Localization of cardiac related changes in the thorax, *Clin. Phys. Physiol. Meas.* Vol. 8, Suppl. A, 167-173, 1987

[6] Y. F. Mangnall, A. J. Baxter, R. Avill, N. C. Bird, B. H. Brown, D. C. Barber, A. D. Seagar, A. G. Johnson, N. W. Read, Applied Potential Tomography: a new non-invasive technique for assessing gastric function, *Clin. Phys. Physiol. Meas.* Vol. 8, Suppl. A, 119-129, 1987

[7] F. J. McArdle, Investigation of cardiosyncronous images of the heart and head using applied potential tomography, Ph. D. thesis, Sheffield: University of Sheffield, 1992

[8] J. Conway Electrical Impedance Tomography for thermal monitoring of hyperthermia treatment: An assessment using in vitro and in vivo measurements, *Clin. Phys. Physiol. Meas.* Vol. 8, Suppl. A, 141-146, 1987.

[9] K. G. Boone, A. M. Lewis, D. S. Holder, Imaging of cortical spreading depression using EIT: Implication of localization of epileptic foci, *Physiol. Meas.* Vol. 15, Suppl. 2A, A189-A198, 1994

[10] H. P. Schwan and C. F. Kay, The Conductivity of Living Tissues, *Ann. N.Y. Acad. Sci.* 65:1007, 1957.

[11] S. Rush, J. A. Abildskov and R. McFee, Resistivity of Body Tissues at Low Frequencies, *Circulation Res.*, 12:40, 1963.

[12] R. Pethig, Dielectric properties of body tissues, *Clin. Phys. Physiol. Meas.* Vol. 8, Supp. A, pp. 5-12, 1987

[13] B. Rigaud, J. P. Morucci, Bioelectrical Impedance Techniques in Medicine. Part III: Impedance Imaging, First Section: General Concepts and Hardware, *Crit. Rev. Biomed. Eng.* ed. John Bourne, Vol. 24, Issues 4-6, pp. 467-588, 1996

[14] M. S. Hamalainen and J. Sarvas, Realistic Conductivity Geometry Model of the Human Head for Interpretation of Neuromagnetic Data, *IEEE Tran. on Bmed. Eng.*, Vol. 36, No. 2, Feb. 1989.

[15] R. S. MacLeod and D. H. Brooks, Recent Progress in Inverse problems in Electrocardiography, *IEEE EMB Magazine*, Vol. 17, No 1, Jan. /Feb.1998.

[16] P. P. Tarjan, and R. McFee, Electrodeless Measurements of the Effective Resistivity of the Human Torso and Head by Magnetic Induction, *IEEE Trans. Biomed. Eng.* Vol. 15, No:4, October 1968.

[17] P. P. Tarjan Electrodeless Measurements of Resistivity Fluctuations in the Human Torso and Head, Ph. D. thesis, Syracuse: Syracuse University, 1968

[18] J. R. Wait, *Geo-Electromagnetism*, Academic Press, New York, 1982.

[19] W. R. Purvis, R. C. Tozer, D. K. Anderson, I. L. Freeston, Induced Current Impedance Imaging, *IEE Proc.* , pt. A, Vol. 140, No:2, pp. 135-141, March 1993.

[20] N. G. Gencer, Electrical Impedance Tomography Using Induced Currents, Ph. D Thesis, Middle East Technical University, 1993

[21] N. G. Gencer, M Kuzuoglu, and Y. Z. Ider, Electrical Impedance Tomography Using Induced Currents, *IEEE Trans. Med. Imag.*, Vol. 13, No:2, pp. 338-350, June 1994.

[22] N. G. Gencer, Y. Z. Ider, and S. J. Williamson, Electrical Impedance Tomography: Induced Current Imaging Achieved with a Multiple Coil System, *IEEE Trans. Biomed. Eng.* Vol. 43, No:2, pp.139-149, February 1996.

[23] M. N. Tek and N. G. Gencer, A new 3D FEM formulation for the Solution of Potential Fields in Magnetic Induction Problems, *IEEE EMBS 19th Annual International Conf.*, 1997.

[24] I. L. Freeston, R. C. Tozer, Impedance Imaging using Induced Currents, *Physiol. Meas.* Vol. 16, (suppl. 3A), pp. 257-266.

[25] K. Boone, D. Barber, B. Brown, Imaging Resistivity with Electricity: Report of the European Concerted Action on Impedance Tomography, *Journ. Med. Eng. & Tech.* Vol. 21, No: 6, pp. 201-232, 1992.

[26] S. G. Davids, Evaluation of applied potential tomography: a clinician's view, *Clin. Phys. Physiol. Meas.* Vol. 8, Supp. A, 175-180, 1987.

[27] Y. Z. Ider, M. Kuzuoglu, B. Nakiboglu, N. G. Gencer, Determination of the Boundary of an Object Inserted Into a Water-Filled Cylinder, *Clin. Phys. Physiol. Meas.* Vol. 13, Supp. A, pp. 155-159.

[28] J. P. Morucci, B. Rigaud, Biolectrical Impedance Techniques in Medicine, In John R. Bourne, Editor, *Crit. Rev. Biomed. Eng.* Vol. 24 (4-6), 655-677, 1996

[29] R. Plonsey, R. Collin, Principles and Applications of Electromagnetic Fields, McGraw-Hill Book Company, New york, 1961

[30] D. K. Cheng, Field and Wave Electromagnetics, Addison-Wesley Publication Company, Inc. 1989

[31] E. E. Kriezis, T. D. Tsiobukis, S. M. Panas, J. A. Tegopoulos, Eddy currents: Theory and applications, *Proc. IEEE* Vol. 80, pp. 1559-1589, 1992

[32] S. Webb, The Physics of Medical Imaging, IOP Publishing Limited, Bristol, 1988

[33] H. Griffiths, A. Ahmed, A dual fequency applied potential tomography technique: computer simulations, *Clin. Phys. Physiol. Meas.* Vol. 8, Supp. A, pp. 103-107, 1987

[34] H. Griffiths, H. T. L. Leung, R. J. Williams, Imaging the complex impedance of the thorax, *Clin. Phys. Physiol. Meas.* Vol. 13, Supp. A, pp. 77-81, 1992

[35] M. E. Valentinuzzi, Bioelectrical Impedance Techniques in Medicine. Part I: Bioimpedance Measurement. First Section:General Concepts, *Crit. Rev. in Biom. Eng.* Vol. 24, Issues 4-6, pp. 223-255, 1996.

[36] A. Ghahary, Electrical Safety, *Electrical Impedance Tomography* Ed: J. G. Webster, pp 58-69, IOP Publishing Ltd., Bristol, 1990.